Journal of Power Sources 261 (2014) 198–205

Contents lists available at ScienceDirect

Journal of Power Sources

journal homepage: www.elsevier.com/locate/jpowsour

On the accuracy of triple phase boundary lengths calculated from tomographic image data

Peter S. Jørgensen [a,*], Kyle Yakal-Kremski [b], James Wilson [b,1], Jacob R. Bowen [a], Scott Barnett [b]

[a] Department of Energy Conversion and Storage, Technical University of Denmark, Risø Campus, Frederiksborgvej 399, 4000 Roskilde, Denmark
[b] Department of Materials Science, Northwestern University, Evanston, IL 60208, USA

HIGHLIGHTS

- A detailed breakdown of the causes of TPB calculation errors and expected accuracy.
- A multitude of approaches used both synthetic tests and real microstructure.
- Comparison between two different methods previously used in literature.
- Identification of possible systematic errors in TPB calculations.

ARTICLE INFO

Article history:
Received 9 December 2013
Received in revised form
27 February 2014
Accepted 10 March 2014
Available online 26 March 2014

Keywords:
Triple phase boundary
Accuracy
Solid oxide cell
Tomography
Microstructure

ABSTRACT

The triple phase boundary (TPB) length is one of the most important quantities obtainable from three dimensional reconstructions of solid oxide fuel cells that utilize porous composite electrodes. However, the choice of TPB calculation method and the voxelation of the microstructures can lead to systematic errors in TPB estimates. Here, two approaches for calculating the TPB density are compared to investigate how different TPB aspects such as curvature, orientation, and phase contact angles affect the results. The first approach applies a correction factor to the TPB length calculated by simply summing voxel (volume element) edge lengths that are shared between voxels of three different phases. The second approach applies a smoothening technique to the TPB curves. The two methods are compared by calculations on different kinds of artificially generated microstructures and on a real SOFC electrode microstructure obtained by focused ion beam tomography. Results are presented showing how specific aspects of different microstructures affect the TPB length calculation error.

1. Introduction

In solid oxide fuel cell (SOFC) and solid oxide electrolyzer cell (SOEC) electrodes, the microstructure of the constituent phases can be correlated to the performance of that electrode [1]. Analysis of the microstructure by 3D tomographic methods such as focused ion beam tomography [2–6] and X-ray tomography [7–9] has seen extensive activity within the past decade. One of the most important parameters that can be calculated from 3D image data is active site density, quantified by the triple phase boundary (TPB) length for most composite electrodes without a mixed ion–electron conductor phase. 3D analysis is arguably the best method to obtain accurate, quantitative values for TPB length, as it typically provides data from large enough volumes to provide good statistical accuracy [4] and the connectivity of the TPB sites can be determined directly [2]. Many different approaches have been used to calculate the TPB length from 3D images [10–13] but only limited analysis [12–14] has been made of the expected accuracy of the calculations compared to the real physical length in the sample.

This paper focuses on the effects that discretization of the physical microstructure into voxels, an inherent result of all imaging processes, has on TPB length calculations. While there might be considerable errors associated with image processing and segmentation [15,16] these effects are very challenging to quantify, since the "true" structure is not known, and are not discussed here. An analysis of the errors that can be expected when calculating the TPB length from voxel image data is presented, comparing two different calculation methods. Two different approaches are taken

* Corresponding author. Tel.: +45 46775672.
E-mail addresses: psjq@dtu.dk, peterstanleymusik@yahoo.dk (P.S. Jørgensen).
[1] Present address: Bloom Energy, 1299 Orleans Drive, Sunnyvale, CA 94089, USA.

http://dx.doi.org/10.1016/j.jpowsour.2014.03.078
0378-7753/

to examine how accurate the two calculations are for different TPB curve shapes. First, calculations are performed on artificial microstructures where the exact analytical TPB length is known. The artificial structures allow for a detailed analysis of how different aspects of the TPB curves affect the accuracy of the calculations using geometrical primitives that attempt to isolate specific aspects of the TPB curves. Second, the two calculations are compared on a 3D reconstruction of a real microstructure.

2. Methodology

2.1. Definition of a TPB segment

Composite solid oxide fuel cell electrodes are comprised of three phases: an ion conducting solid phase, an electron conducting solid phase, and pores containing the gas phase. TPB lines, defined by the intersections where the three phases meet, are usually considered to be the electrochemically active regions of the electrode. The TPB lines must form closed curved loops. To see this, consider two particles pressed together to form a surface interface. If these particles are suspended in a third, matrix phase, the TPB line will be a closed curve defined by the perimeter of the particle–particle interface.

Unfortunately, much of the information about the curvature and exact location of the physical TPB curve is irrevocably lost by discretization to a raster format during image data acquisition. The data, represented as a 3D image, can be described as identical cuboid volume elements (voxels) arranged in a regular ordered 3D grid. Each voxel face is shared by two neighbors, each voxel edge is shared by 4 neighboring voxels and each voxel vertex is shared by 8 neighboring voxels. Using this description a TPB segment can be defined as an edge that is shared by a voxel of at least one of each phase. By this definition, a TPB segment can only be aligned along three directions and can only have three discrete lengths corresponding to the x, y and z side lengths of a voxel.

In the above description, TPB lines coincide with voxel edges, but in real electrodes TPBs can have any orientation relative to the voxel edges. This results in an over-estimation of the TPB length except for cases where the line segment lies directly along one of the voxel edges. At worst, a TPB line segment will pass through the diagonal of the voxel cuboid, resulting in a local overestimation of the length by a factor of $3/\sqrt{3} \approx 1.732$. If the line segment passes along a face diagonal, the local overestimation will be by a factor of $2/\sqrt{2} \approx 1.414$.

It follows that if the total TPB length is calculated by simply summing the length of all TPB segments in the voxel cuboid, an overestimation of the total TPB would result. We denote this raw unmodified TPB length TPB_{raw}. In this work two different approaches to obtaining a better estimate of the total TPB length are studied: a correction factor approach and a curve smoothing approach.

2.1.1. The correction factor approach

The overestimation in TPB length can be corrected provided TPB curve sections can be accurately approximated as straight line segments on the size scale of a voxel, and that there is no systematic texture or alignment of TPB lines or particles in the sample. A correction factor has been calculated by performing a surface integral over a sphere octant on the sum of 3D components defining a sphere radius ($\rho = 1$) divided by the line segment length derived from the Pythagorean Theorem. This is then normalized by a surface of the sphere octant. The overestimation factor of $(\pi/2 + 3)/\pi \approx 1.455$ (denoted TPB_{cf}) is reached, as shown in Wilson et al. [17]. To obtain the TPB length estimate, the total raw TPB length is simply divided by this factor.

2.1.2. The curve smoothing approach

This approach, as described in detail in Jørgensen et al., [12] (the voxel precision version) seeks to obtain an accurate estimate of the TPB length by moving the vertex position of the TPB segments to obtain a smoother TPB curve. The method keeps track of the connectivity of the TPB curve loops and it is thus possible to perform a simple smoothing operation on the vertex position of the connected TPB segments by a weighted average of neighboring vertex positions. A simple weighting scheme is used which repositions each vertex on the TPB curve with a weight of 0.5 to the vertex itself and a weight of 0.25 to its two neighbors in the loop. Additional smoothing can be introduced by performing the smoothing operation more than once. For this work, one and two smoothing iterations have been used and results from these methods are denoted TPB_{s1} and TPB_{s2} throughout the text. Two iterations have typically been used when performing calculations on real microstructures using this method – results for the one smoothing iteration are included here only to indicate what effect the number of smoothing iterations has.

The centroid method used in other work [18,19] is essentially very similar to the smoothing scheme described above since the new vertex position is located at the center of the triangle created by the midpoints of three neighboring TPB segments.

2.2. Solid oxide fuel cell electrode microstructure

A real SOFC cathode structure is analyzed by both the correction factor and the curve smoothing approach. The cathode consists of $(ZrO_2)_{0.92}(Y_2O_3)_{0.08}$ (YSZ), $(La_{0.8}Sr_{0.2})_{0.98}MnO_{3-\gamma}$ (LSM), and pore phase; these are the ion, electron, and gas transport phases, respectively. Processing was done similarly as described by Cronin et al. [4]. However, a 96 h, 1000 °C anneal was done in air before application of the current collector. Tomographic data was collected on a Zeiss NVision 40, using an electron backscatter detector to increase contrast between each phase as described elsewhere [4]. The total reconstruction volume is $6.3 \times 12.0 \times 10.3$ μm, with a x–y resolution of 15 nm, and a z resolution of 30 nm, which corresponds to a voxel cube of $420 \times 800 \times 342$ voxels. An orthogonal slice view of the segmented data set can be seen in Fig. 1.

2.3. Artificial microstructures

To be able to quantify errors in the calculation methods, microstructures with known TPB lengths are required. The exact TPB length is however not obtainable experimentally from real electrodes. As an alternative, TPB calculations have been performed on two types of artificial microstructures, for which the exact analytical TPB length is known.

2.3.1. Full microstructures

The TPB length calculations were done on a set of artificial microstructures consisting of packed overlapping spheres, which resemble real 'partially sintered' particle microstructures, as reported by Metcalfe et al. [14]. Due to the simplistic nature of these microstructures, they do not have a realistic distribution of TPB curve orientations and curvatures. As will be shown below, this affects the results greatly. The microstructures do, however, provide a sanity check for the overall accuracy of the methods on microstructures that are of similar size and phase distribution as a real microstructure.

2.3.2. Geometrical primitives

Simple test geometry is used to investigate the influence of different aspects of the TPB curve on the accuracy of the calculation methods. This setup is an extension of the methods applied in Refs.

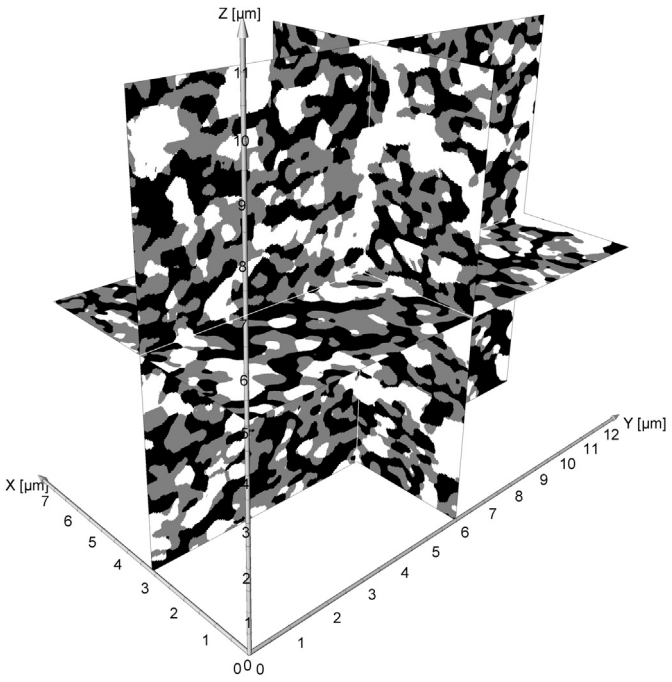

Fig. 1. Orthogonal slice representation of the real SOFC microstructure after segmentation. Black structures correspond to pores, gray structures to YSZ and white structures to LSM.

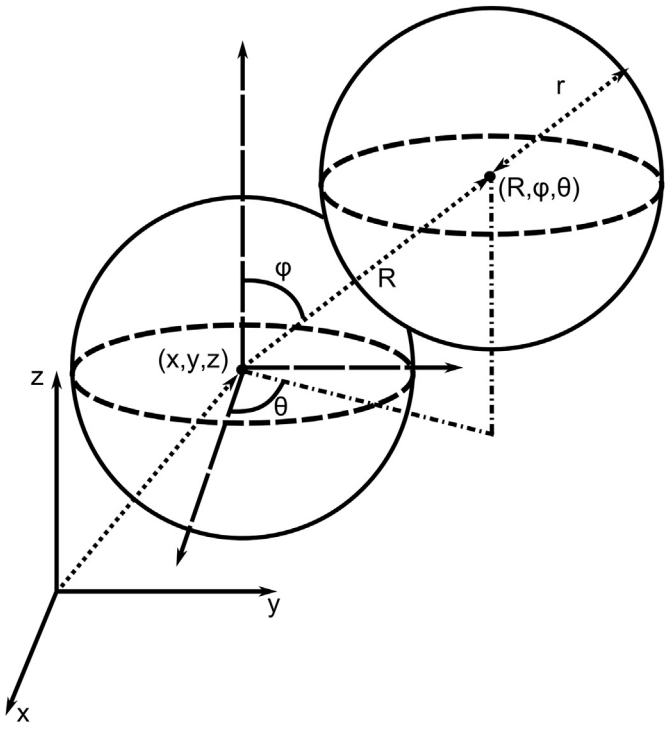

Fig. 2. The two sphere setup. The first sphere is placed relative to the center of an arbitrary voxel in Cartesian coordinates. The second sphere is placed relative to the first sphere in spherical coordinates.

[12,13]. It allows the different characteristics of the TPB curve to be analyzed such as curvature, orientation and the contact angle between the three phases.

The test geometry consists of two intersecting spheres, each of radius r, with centers a distance R from each other. Thus, the exact analytical TPB length (the circumference of the circle defining the sphere–sphere interface) can be calculated as $\mathrm{TPB_{anal}} = 2\pi\sqrt{(r^2 - (R/2)^2)}$. Relative errors calculated below are thus calculated as the signed relative deviation from this value e.g. $(\mathrm{TPB_{cf}} - \mathrm{TPB_{anal}})/\mathrm{TPB_{anal}}$.

Several other parameters concerning the orientation and placement of the sphere–sphere body in a voxel grid can be controlled; the x, y and z coordinate offset of the first sphere center relative to the center of a voxel (equivalent to the offset from the origin of the coordinate system); the displacement vector of the second sphere center relative to the first in spherical coordinates ($\rho = R$, θ, φ). Note that changing x, y, z resolution is equivalent to changing sphere size, so only the sphere size was changed. The setup is illustrated in Fig. 2.

The construction of a perfect voxel cube segmentation of the two-sphere geometry is straightforward. The two sphere centers are calculated using a certain parameterization (R, x, y, z, θ, φ). First, the location of the first sphere is determined by the x, y and z offset. Second, the location of the second sphere is determined based on its displacement vector (θ, φ) and distance to the first sphere (R). The location of the second sphere is thus dependent on the location of the first sphere. Each voxel in a voxel cube is then assigned to either sphere/phase one or sphere/phase two depending on which sphere center it has the shortest Euclidian distance to. If both distances are greater than r then the voxel is assigned to the third phase. The x, y and z offsets are introduced to avoid situations where voxel centers have the exact same distance to both spheres and to avoid discretization artifacts introduced by perfect alignment of sphere centers with voxel centers.

TPB curves in real electrodes are unlikely to be perfect circles. However, the idea here is that a real physical TPB curve can be thought of as consisting of a combination of arcs with constant radius, each with different curvature and orientation. By analyzing the results from the sphere tests, trends in the TPB calculation error – introduced by different TPB curve characteristics – can be investigated to better understand what is causing the discrepancies. All calculations using this setup are performed unit less with an isotropic voxel size of 1.

3. Results and discussion

The two sphere setup is used to assess the effect on the TPB length correction of the curve orientation (Section 3.1), TPB curvature (Section 3.2), and contact angle (Section 3.3). In Section 3.4, the convergence of the TPB correction is assessed, again in the two sphere model. The relative errors of the different TPB calculation methods are then compared for an idealized packed-sphere microstructure (Section 3.5) and a real microstructure (Section 3.6). General implications of the results are discussed in Section 3.7.

3.1. Effect of curve orientation

Fig. 3A shows the calculated correction factor needed to match the raw TPB length with the analytical TPB length, with varying offsets of the first sphere and varying orientations of the second sphere relative to the first (see Fig. 2). In these results, the sphere diameter and inter-sphere distances r and R are set at 20 (geometry defined in Fig. 2). For reasons of symmetry an octant of a sphere is gridded 10 by 10 in θ and φ with values in the range $[0{:}\pi/2]$. The black points in Fig. 2 show the end location of the vector describing the orientation the second sphere relative to the first. The vectors are shown on a unit sphere in Cartesian coordinates (Note the distinction between the X, Y and Z axes in this plot and the two sphere model parameters x, y and z). For each of these orientations the value at the black points is the average of 50 calculations made

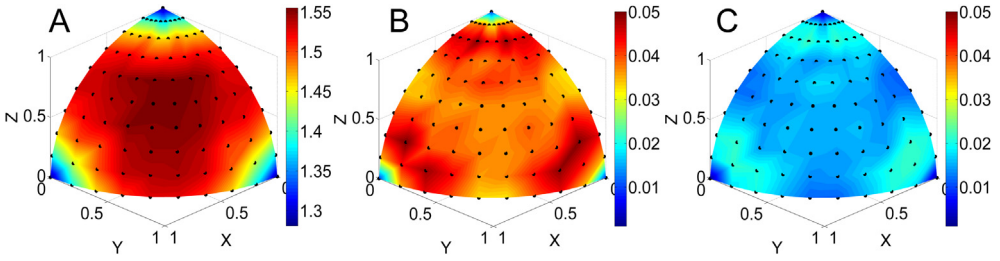

Fig. 3. The effect of curve orientation. (A) The correction factor needed to match the analytical TPB length. (B) The relative error with one smoothing iteration. (C) The relative error with two smoothing operations.

with a random x, y and z offset to the center of the first sphere in the range [−0.5:0.5]. Since sphere two is placed relative to sphere one the same offset indirectly applies to sphere two as well. This random offset is introduced to remove any artifacts resulting from the alignment of sphere centers with voxel centers. The values between the black points in Fig. 2 are interpolated.

The correction values range between 1.281 at the corners of the plot (i.e., with the sphere centers aligned along a x, y, or z axis of the voxels), and 1.555 at the center of the plot, corresponding to the voxel diagonal. These values correspond to relative errors of −11.95% and 6.88% respectively if the TPB_{cf} correction factor had been used at all orientations. This is a significant difference, but note that the correction factor for the TPB_{cf} method in actual structures is derived as an average over a large number of directions and not for one specific direction. Additionally, the very low correction factors are only present in a small region around the aligned directions and the majority of the possible orientations have correction factors in the 1.45–1.55 range.

Fig. 3B and C shows the relative error of the smoothing method with one and two smoothing iterations, again using the two-sphere model. The TPB_{s1} estimate varies between an error of 0.86% and 5.00% compared to the analytical value and the TPB_{s2} between 0.1% and 2.22%. Since these methods smooth the TPB curve before calculating the length they are much less affected by the orientation of the curve. Some systematic trends are, however, still visible. The TPB_{s2} method has significantly lower variation than the TPB_{s1} method and gives an accurate estimate of the TPB length at all orientations. This is not surprising since the smoothing by the TPB_{s2} method is based on a weighted average of 5 vertices rather than 3 and thus creates smoother curves. As will be shown below, this also means that some TPB curve shrinkage is inevitable.

In a typical real microstructure of significant size, the TPB_{cf} and TPB_{s2} methods are expected to both have low errors due to curve orientation. However, if the measured volume is small or some anisotropy in the microstructure results in an anisotropic distribution of TPB curve orientations, the use of a correction factor method could result in significant error.

3.2. Effect of TPB curvature

To quantify the effect of curvature the TPB radius of curvature relative to the voxel side length (ν) is introduced. This normalized TPB radius is then calculated using the two sphere setup. The sphere diameters are set equal to the inter-sphere distance for all tests ($r = R$). The x, y and z offsets are chosen randomly in the range [−0.5:0.5] and θ and φ are chosen randomly in the range [0:π/2]. 200 random configurations of x, y, z, θ and φ are evaluated for each value of $r = R$ (in the range 0–18).

Fig. 4 shows a plot of the average error of each method relative to the analytical TPB length, versus ν. All calculation methods yielded a 100% underestimation for $\nu < 0.5$, not surprising since each sphere is smaller than a voxel and hence cannot be represented by a voxel structure. The large error in the range from $\nu = 0.5$–1.5 results because the TPB circles are represented by the same voxel structure – a simple rectangle – obviously a poor representation of a circle. Considering the loss of information about the size of the real TPB curve, both the TPB_{cf} and the TPB_s methods are equally affected. For ν increasing from 1.5 to 4, the TPB_{cf} method converges faster to the correct value than the TPB_{s1} and TPB_{s2} methods, where there are too few vertices to accurately smooth and represent the true TPB. For larger ν, all methods converge but retain small positive errors. For example, at the largest calculated ν value of 17.94 the relative errors for the TPB_{cf}, TPB_{s1} and TPB_{s2} methods are 2.77%, 3.88% and 1.66%, respectively.

The poor representation of circles affects the two methods somewhat differently. The correction factor method assumes that the TPB curve segments are randomly oriented straight lines. For large radius of curvature of the TPB curve this is a good approximation but for small radius of curvature the approximation of a curve by a line leads to underestimation of the length. The TPB_s methods are theoretically also only accurate on straight lines but are affected much more severely by high curvature than the correction factor method. Due to the smoothing by weighted neighbor averages the smoothing of TPB curves consisting of few vertices (i.e. if we consider a simple rectangle) results in a severe shrinkage of the TPB curve after vertex repositioning, collapsing to a point if enough smoothing iterations are applied.

To assess whether the radii in a real microstructure are small enough to produce significant errors, the distribution of the radii of curvature was determined. The angles between the TPB line segments obtained from the TPB_{s2} method were obtained. The angles

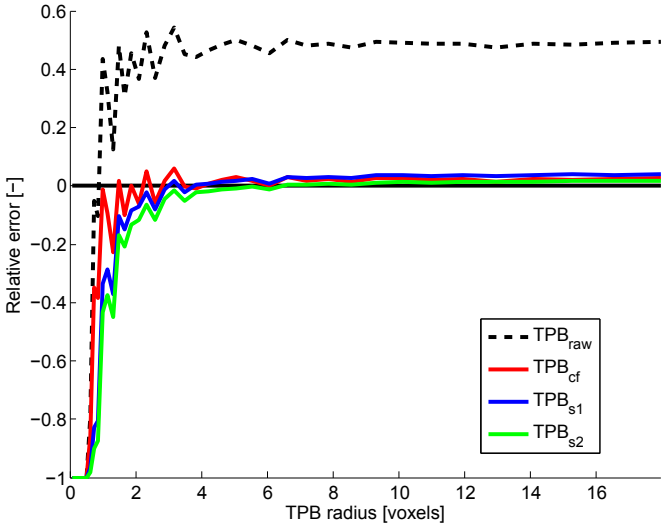

Fig. 4. The effect of TPB curvature.

were then converted to their corresponding radii of curvature and normalized by the average voxel side length of 20 nm. The TPB_{s2} line segments are derived from smoothing the original voxelated TPB segments and are thus only an estimate of the distribution in the real microstructure. The distribution of the radius of curvature in the real microstructure (described in Section 2.2) is shown in Fig. 5. A significant fraction of the TPB segments in the real microstructure have $\nu < 4$. In this data, the voxel size was $15 \times 15 \times 30$ nm and the average feature size was 300 nm, 250 nm and 440 nm for pores, YSZ and LSM (calculated as the D50 of the continuous PSD [20]). This ratio of the feature size to the voxel size would normally be considered large enough for good statistical accuracy [4]. Although $\nu < 4$ seems small for this case, the TPB curves don't always have uniform circle-like curvature, but rather twist and bend in all directions yielding locally small ν values.

3.3. Effect of contact angle

The contact angle ξ of the three phases at the TPB sites also affects the accuracy of the TPB calculations (see Fig. 6). This is an artifact of the voxelation of the microstructure. As the contact angle between two of the phases becomes small the structure of the intervening third phase becomes long and narrow near the TPB. To get accurate measurements of the TPB length, the TPB sites must be identified at the end of this long narrow structure indicated by the white voxels in Fig. 6. However, due to the voxels having finite size the narrow structure cannot be well defined by the voxel structure and the narrow structure is thus likely to be filled by one of the other phases. The end result is that the TPB sites in the voxel structures are shifted away from the true TPB sites. The analysis performed below is based on the contact angle between intersecting spheres and is made to illustrate the possible magnitude of this effect. The effect on the two intersecting spheres will always be an overestimation of the TPB length due to the TPB line being pushed outwards away from the circle intersection of the two spheres.

To quantify the effect of the contact angle the two sphere setup is used. A range of contact angles are chosen and the corresponding r and R values are calculated such that the analytical TPB length is kept constant at 17.32 and only the contact angle is changed. For this test the x, y and z offset are set to 0 and the same θ, φ grid is used as in the curve orientation set resulting in 100 experiments for each contact angle.

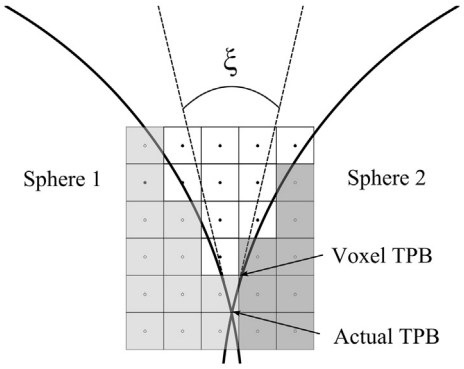

Fig. 6. Illustration of the contact angle ξ in the two sphere setup, defined here as the angle between the tangents of the two spheres where they intersect. A voxelization of the area around intersection between the two spheres is overlaid to illustrate the voxelization issue at low contact angles. The voxels are color coded according to which part of the figure their centers cover. Note the discrepancy between the TPB location for the voxel structure and the true TPB location at the sphere intersection.

Fig. 7 shows a plot of the relative errors for the mean of 100 experiments as a function of the contact angle. The trend is similar for all the methods; high positive relative error is observed at low contact angles followed by a decline towards smaller relative error at a contact angle of 120°. At 60° contact angle the relative errors for TPB_{cf}, TPB_{s1} and TPB_{s2} are 4.84%, 7.64% and 4.63%, respectively, and for 120° the errors are 0.14%, 3.38% and 1.30%.

3.4. Convergence rate

A good 3D microstructure measurement should observe a large enough volume to minimize errors in the derived quantities, e.g. TPB length, due to random variations. As has been shown above, variations in orientation and curvature of the TPB curves affect the accuracy in different ways, but when an actual structure is considered in aggregate, the variations may tend to cancel and the errors thus become minimal. Here we consider the precision of the TPB estimates by repeatedly calculating the total TPB line length of a large number of individual curves.

The two sphere setup is utilized again, with 2000 experiments run with r set to 25 and all other parameters randomly selected; x, y

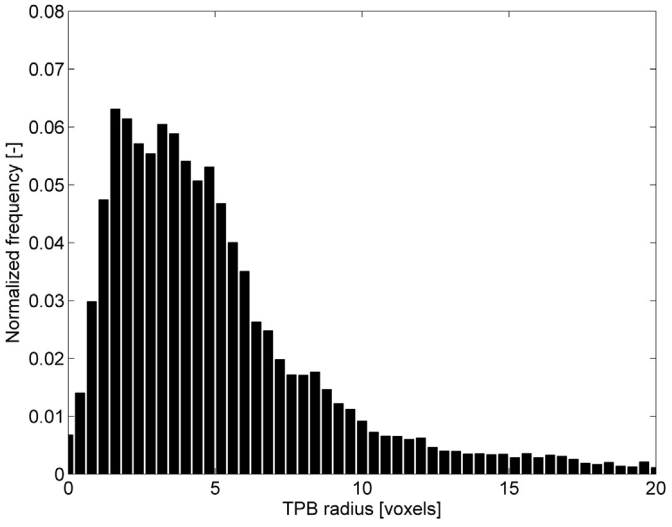

Fig. 5. The calculated distribution of local radius of curvature for the real SOFC microstructure using the line segment output of the TPB_{s2} method.

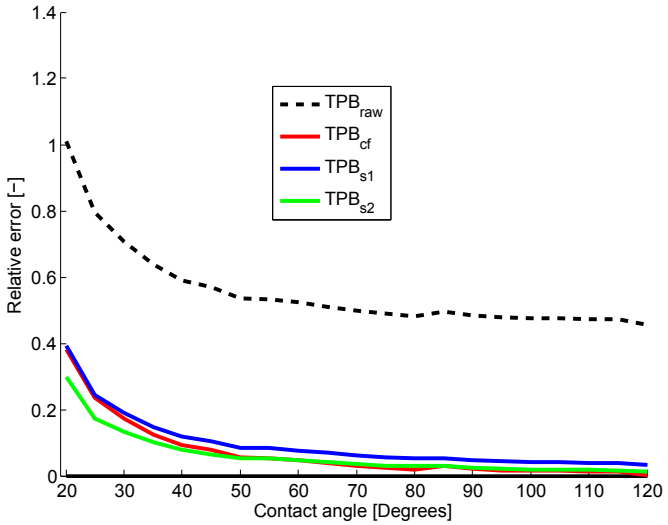

Fig. 7. The effect of contact angle.

and z in the range [−0.5:0.5], θ and φ in the range [0:π/2] and R in the range [12.5:37.5]. An amount M (the averaged amount in Fig. 8) of the 2000 experiments is selected randomly and their average TPB estimation error compared to the analytical value is calculated. The procedure of randomly picking M experiments from the 2000 is repeated 1000 times and the standard deviation σ of the average TPB error over the 1000 repetitions is calculated. This procedure is then repeated for a range of M. Since a random selection of the same 2000 experiments are repeatedly used this methodology of estimating σ obviously breaks down as M becomes a large fraction of the 2000 experiments since each random selection of experiments will have an increasing number of already included experiments.

Fig. 8 shows $\pm 1.96\sigma$ (95% confidence interval for normally distributed data) ranges for each of the methods with the relative error of the average of all 2000 experiments subtracted. The TPB_{cf} method has significantly slower convergence rates than the TPB_s methods. This is as expected since the TPB_{cf} factor is derived to only hold when averaged over all directions. The relative errors averaged over all 2000 experiments are 3.73%, 4.25% and 1.89% for the TPB_{cf}, TPB_{s1} and TPB_{s2} respectively.

A correction factor of 1.5092 is needed in this test to match the total analytical TPB length of the 2000 tests with the TPB_{raw} estimate. This is slightly different than the theoretically derived correction factor of 1.455 noted above for the TPB_{cf} method. However, keep in mind that the numerically derived correction factor of 1.5092 is obtained by choosing a specific distribution of TPB parameters. That is, the estimated correction factor of 1.5092 only holds for this particular distribution of TPB curve parameters.

As seen in the previous sections, some of the effects of the TPB curve parameters shift the TPB estimate in different directions; increasing curvature results in under-estimation for all the methods and decreasing contact angle results in an under- or over-estimation depending on direction of the smallest contact angle. Since the relative errors are not constant across all the parameter tests, it is not possible to give a simple adjustment factor to each method that would universally increase the accuracy for all microstructures.

3.5. Pseudo realistic microstructure

Fig. 9 shows the relative errors obtained by each method on five random artificial microstructures generated using the same input parameters. For this analysis the two sphere model was not used but rather the pseudo realistic structures describe in Section 2.3.1. The artificial microstructures are generated with particle centers positioned on a face centered cubic lattice. The randomness in the five microstructures comes from the random assignment of phase (or pore) to each lattice point. The characteristic structure has the effect of creating TPB lines only on a few specific planes, either parallel to the voxel faces, through diagonal voxel edges or through diagonal voxel vertices (see Ref. [14] for details). Thus, this "pseudo-realistic" structure is subject to the same effects as delineated above using the two-sphere geometry, but here multiple TPB curves are arranged in a more realistic way in the same microstructure. Fig. 9 shows a discrepancy between the TPB_{cf} and TPB_{s1} results and the TPB_{s2} results, presumably for the same reason as those shown in Fig. 3, where the TPB_{cf} and TPB_{s1} methods both obtain higher estimates than the TPB_{s2} method in these directions. The increased variation in error for the TPB_{cf} method is likely a result of the TPB curves in the microstructure all lying in a few discrete planes thus resulting in poor sample statistics for the TPB curve orientation. All the methods show errors less than 3% in magnitude as expected from the large radius of curvature ($\nu > 20$) and contact angle ($\xi > 90°$) of the TPB curves in the structure.

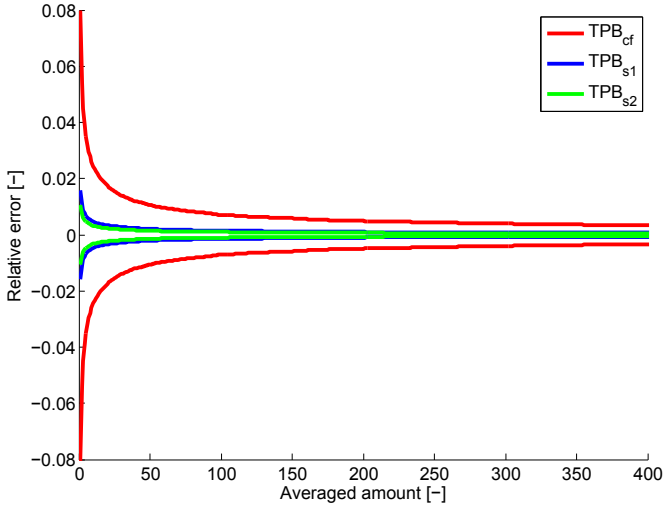

Fig. 8. TPB convergence. The standard deviation of the average error as a function of the amount of TPB curve loops averaged over.

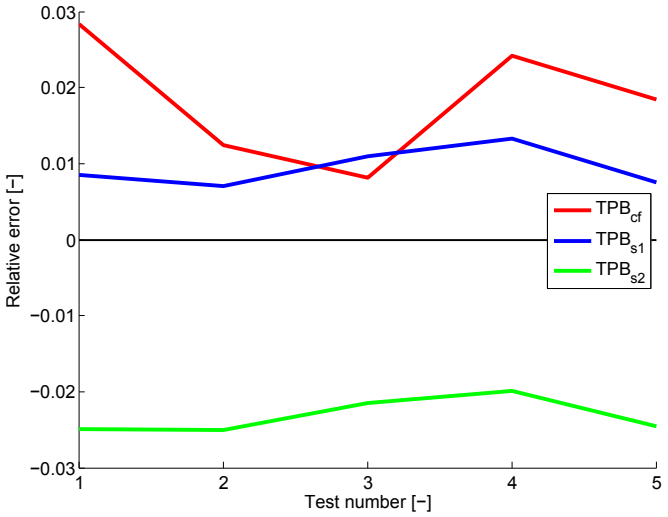

Fig. 9. The results of 5 realizations of the same artificial microstructure.

3.6. Real microstructure

The results of the TPB length calculations on the real SOFC microstructure can be seen in Table 1. An orthogonal slice view is shown in Fig. 1. The TPB_{cf} and TPB_{s2} methods that have previously been used to analyze real microstructure [3,4,12,17,21] have a relative difference of 4.02% (calculated as the absolute difference between the two divided by their average). As shown in Fig. 5 low radius of curvature is frequently observed, indicating that the shrinkage effect is the main cause of the discrepancy as previously shown in Fig. 4.

Table 1
TPB estimates calculated using 3 different methods. The relative differences are calculated as the deviation from the mean of the 3 estimates.

Measuring method	TPB value [μm μm^{-2}]	Relative difference [%]
Correction factor	11.42	1.15
Curve smoothing 1 iter.	11.48	1.66
Curve smoothing 2 iter.	10.97	−2.83

Recall that the TPB calculation error can be affected in opposite directions based on the nature of the TPB curve. These errors will under some circumstances cancel each other out and under other circumstances skew the results in a specific direction. The circumstances are however microstructure- and imaging-method-dependent, and it cannot be easily determined to what degree these errors are present, both for the present image and in general. On the other hand, the differences between results obtained using different methodologies can help hint at specific properties of the TPB curves that could skew the result in a certain direction.

3.7. Implications of the results

It is not possible to determine the true accuracy of current TPB calculation methods. The error is dependent on the microstructure under investigation and depends on both the orientation, curvature and contact angle of the TPB curves. Increasing image resolution will reduce errors due to curvature and contact angle. Increased sample size will reduce errors due to TPB curve orientation since the value is averaged over a larger amount of random orientation. The results of the two sphere tests under various conditions indicate that for sufficiently high resolution (high TPB radius of curvature) and contact angle both the TPB_{cf} and the TPB_{s2} methods generally overestimate the TPB length by 1–3%, as indicated in Figs. 4 and 7. There is always a tradeoff between voxel resolution and the physical size of the reconstructed volume. This means that increasing the voxel resolution to a domain with only high radii of curvature for the TPB curves is not always possible or practical.

The correction factor method and the smoothing method were shown to have a relative difference of 4.02% on a large real sample obtained by FIB tomography. This discrepancy is large enough that the same method should always be used when conducting comparative studies of microstructure evolution but is also low enough that it does not matter which of the methods are used as long as the shortcomings of each method are taken into consideration. Running the calculations on both a curve smoothing and a correction factor method can give additional insight into potential inaccuracies.

Both the contact angle and curvature results show a large systematic shift in the error for increased contact angles and radii of curvature (Figs. 4 and 7). This has important implications for studies of microstructure evolution. As an example consider a sintering study where changes to the necking between particles could result in a change in the typical contact angle at the TPB. From Fig. 7 such a change in the contact angle would systematically shift the estimated TPB length, not because of an actual change in the true TPB length but due to changes to the properties of the TPB curve itself. This means that any calculated TPB length changes in such a study will contain both the contribution from the actual change and the contribution from the systematic shift in TPB error due to the changed TPB curve properties.

A similar shift in TPB error can be expected for studies of particle size evolution where the radius of curvature of the TPB curve will change or by comparing microstructure measurements conducted at different resolution and thus different TPB curvature. In fact, Fig. 4 indicates that if the resolution was double (i.e. going from a typical radius of curvature of 3–6) when comparing one microstructure to another the calculated TPB length of the high resolution microstructure would be on the order of 10% higher, again not due to an actual change in the microstructure itself but due to the imaging parameters. A simple down sampling of the real SOFC microstructure data to effectively double the voxel size resulted in a calculated TPB decrease of 5.8% for the TPB_{cf} method and 8.0% for TPB_{s2}. The down sampling further decreases the already low ν (see Fig. 5) of the data set which is the reason for the large difference in the TPB reduction between the two methods as indicated in Fig. 4.

Several other factors than the TPB calculation method affects the TPB length measurement error. Depending on the material investigated and the microscope used the errors introduced by imaging artefacts, image filters and segmentation is expected to be at least as significant as the TPB calculation method. An error on the order of 5% or less from the TPB length calculation method itself should thus not be of concern.

4. Conclusion

The TPB_{cf} and the TPB_{s2} calculation methods investigated here both have strengths and weaknesses. They are both attractive methods, so long as their weaknesses are taken into consideration when selecting a method to analyze a given microstructure. The correction factor method is prone to errors for small sample size and non-uniform distribution of curve orientations. The curve smoothing method is prone to errors for low resolution where significant underestimation of the TPB length can result due to shrinkage of the TPB curve.

Significant errors can crop up when trying to analyze a microstructure that does not have a typical distribution of TPB curve orientations, curvature and contact angle. Care should be taken when conducting systematic studies of microstructure evolution. Not only will the real TPB length change due to the microstructure changes but the error introduced by the measurement method can also shift due to the change in TPB curve parameters, thus either exaggerating or lessening the measured effects on the TPB length from the microstructure evolution.

Acknowledgments

The authors at Northwestern University gratefully acknowledge financial support from National Science Foundation Ceramics Program DMR-0907639 and travel grant DMR-1052678.

SAB gratefully acknowledges financial support for sabbatical leave in the form of an Otto Mønsted-Guest Professorship and the Danish National Bank.

The authors would like to thank C. Metcalfe for access to the artificially generated microstructure data.

The real electrode data set was collected at the Electron Microscopy Center for Materials Research at Argonne National Laboratory, a U.S. Department of Energy Office of Science Laboratory operated under Contract No. DE-AC02-06CH11357 by University of Chicago Argonne, LLC.

PSJ gratefully acknowledges financial support from the Programme Commission on Sustainable Energy and Environment, The Danish Council for Strategic Research, via the SERC project (www.serc.dk), contract no. 2104-06-0011.

References

[1] C.W. Tanner, K. Fung, A.V. Virkar, J. Electrochem. Soc. 144 (1997) 21–30.
[2] J.R. Wilson, W. Kobsiriphat, R. Mendoza, H. Chen, J.M. Hiller, D.J. Miller, K. Thornton, P.W. Voorhees, S.B. Adler, S.A. Barnett, Nat. Mater. 5 (2006) 541–544.
[3] J.R. Wilson, M. Gameiro, K. Mischaikow, W. Kalies, P.W. Voorhees, S.A. Barnett, Microsc. Microanal. 15 (2009) 71–77.
[4] J. Scott Cronin, K. Muangnapoh, Z. Patterson, K.J. Yakal-Kremski, V.P. Dravid, S.A. Barnett, J. Electrochem. Soc. 159 (2012) B385–B393.
[5] N. Vivet, S. Chupin, E. Estrade, A. Richard, S. Bonnamy, D. Rochais, E. Bruneton, J. Power Sources 196 (2011) 9989–9997.
[6] D. Gostovic, J.R. Smith, D.P. Kundinger, K.S. Jones, E.D. Wachsman, Electrochem. Solid-State Lett. 10 (2007) B214–B217.
[7] Y. Karen Chen-Wiegart, J.S. Cronin, Q. Yuan, K.J. Yakal-Kremski, S.A. Barnett, J. Wang, J. Power Sources 218 (2012) 348–351.
[8] P.R. Shearing, J. Gelb, J. Yi, W.K. Lee, M. Drakopolous, N.P. Brandon, Electrochem. Commun. 12 (2010) 1021–1024.

[9] G.J. Nelson, W.M. Harris, J.J. Lombardo, J.R. Izzo Jr., W.K.S. Chiu, P. Tanasini, M. Cantoni, J. Van herle, C. Comninellis, J.C. Andrews, Y. Liu, P. Pianetta, Y.S. Chu, Electrochem. Commun. 13 (2011) 586–589.
[10] H. Chen, H. Yu, J. Scott Cronin, J.R. Wilson, S.A. Barnett, K. Thornton, J. Power Sources 196 (2011) 1333–1337.
[11] J. Golbert, C.S. Adjiman, N.P. Brandon, Ind. Eng. Chem. Res. 47 (2008) 7693–7699.
[12] P.S. Jørgensen, K.V. Hansen, R. Larsen, J.R. Bowen, J. Power Sources 195 (2010) 8168–8176.
[13] H. Iwai, N. Shikazono, T. Matsui, H. Teshima, M. Kishimoto, R. Kishida, D. Hayashi, K. Matsuzaki, D. Kanno, M. Saito, H. Muroyama, K. Eguchi, N. Kasagi, H. Yoshida, J. Power Sources 195 (2010) 955–961.
[14] C. Metcalfe, O. Kesler, T. Rivard, F. Gitzhofer, N. Abatzoglou, J. Electrochem. Soc. 157 (2010) B1326–B1335.
[15] P.S. Jørgensen, K.V. Hansen, R. Larsen, J.R. Bowen, Ultramicroscopy 110 (2010) 216–228.
[16] B. Munch, P. Gasser, L. Holzer, R. Flatt, J. Am. Ceram. Soc. 89 (2006) 2586–2595.
[17] J.R. Wilson, J.S. Cronin, A.T. Duong, S. Rukes, H.Y. Chen, K. Thornton, D.R. Mumm, S. Barnett, J. Power Sources 195 (2010) 1829–1840.
[18] L. Holzer, B. Münch, B. Iwanschitz, M. Cantoni, T. Hocker, T. Graule, J. Power Sources 196 (2011) 7076–7089.
[19] N. Shikazono, D. Kanno, K. Matsuzaki, H. Teshima, S. Sumino, N. Kasagi, J. Electrochem. Soc. 157 (2010) B665–B672.
[20] B. Munch, L. Holzer, J. Am. Ceram. Soc. 91 (2008) 4059–4067.
[21] J.R. Wilson, A.T. Duong, M. Gameiro, H. Chen, K. Thornton, D.R. Mumm, S.A. Barnett, Electrochem. Commun. 11 (2009) 1052–1056.